# Supporting Information

# Insight into the Crucial Role of Secondary Mineral Phases in the Transfer of Gold Nanoparticles through a Sand Column using Online ICP-MS/spICP-MS Monitoring

*Sylvie Motellier*, Dominique Locatelli, Rémi Bera*

University Grenoble Alpes, Commissariat à l'Energie Atomique et aux Energies Alternatives, DRT/LITEN/DTNM/SEN/Laboratory of Nano-characterization and Nano-safety, 17 Avenue des Martyrs, F-38054 Grenoble, France

*Corresponding author. E-mail: sylvie.motellier@cea.fr

Number of pages: 21

Number of tables: 3

Number of figures: 8

## Experimental

### Chemicals, Sample and Eluent Preparation

Hydrochloric acid (Suprapur grade 30% HCl) and nitric acid (Suprapur grade 65% $HNO_3$) were from Merck (Darmstadt, Germany). The ionic Au (1000 mg $L^{-1}$ in 5% HCl), Pt (1000 mg $L^{-1}$ in 5% HCl), and Y (1000 mg $L^{-1}$ in 2% $HNO_3$) standards were from Sigma-Aldrich (Saint Louis, USA), as well as sodium Bromide (NaBr BioXtra grade 99%). The eluent used for the column assays consisted in $10^{-2}$ M sodium chloride (NaCl BioXtra grade 99% from Sigma-Aldrich) dissolved in ultra-pure (UP) water (Direct-Q3, Millipore, Billerica, USA). Its pH (7.5 +/- 0.5) was adjusted with sodium hydroxide (Suprapur grade 30% NaOH from Merck) and it was filtered through a 0.45 µm membrane (Millipore, Burlington, USA). Citrate-capped gold nanoparticles of 50 nm and 100 nm in diameter (referred to as AuNP-50 nm and AuNP-100 nm) were purchased from BBI Solutions (Crumlin, UK). They are suspended in purified water without preservative and their concentration and size are given by the supplier: 56.8 mg $L^{-1}$, 47 – 53 nm (CV < 8%) for AuNP-50 nm and 56.6 mg $L^{-1}$, 96 – 104 nm (CV < 8%) for AuNP-100 nm. The samples were prepared by dispersing the AuNPs in the eluent, with addition of the conservative tracer (150 µg $L^{-1}$ Br prepared with NaBr), and homogenized by vortex stirring for 10 s. The external standard solution for column experiments consisted in 40 µg $L^{-1}$ Y and 100 µg $L^{-1}$ Pt in a matrix composed of 1% $HNO_3$ and 1% HCl. All solutions/suspensions were prepared by careful weighing (precision +/- 0.1 mg) for accurate concentration.

### Purification of the Sand

The sieved sand (200 µm – 400 µm) was purified to remove its impurities (natural organic matter, metal oxides, clay particles) by successive two-hour steps of dispersion in 1M HCl / $H_2O$

/ 1M NaOH in a 3-dimensional shaker (Turbula from WAB, Muttenz, Switzerland). The protocol was repeated seven times. The sand was further transferred into a column for two cycles of 1M HCl / $H_2O$ / 1M NaOH percolations. It was then rinsed thoroughly with UP water, re-dispersed in UP water, put in an ultrasonic (US) cleaner (Branson, Danbury, USA) for 30 min before the final rinse with UP water. It was finally dried in an oven (Venti-Line, VWR, Radnor, USA) at 60°C and stored in a tight container.

**Characterization Techniques**

Scanning electron microscopy (SEM S5500 from Hitachi, Naka, Japan) with an energy dispersive X-ray spectroscopy (EDS) microanalysis system (Noran from ThermoFisher Scientific, Madison, USA) was used to evaluate the efficiency of the purification steps of the sand. The acceleration voltage was 4 kV to 10 kV depending on the sample. The dry sand was deposited on a carbon adhesive film and Pt-metallization was performed to prevent charging effects. The surface charge of the grains was assessed by zeta potential measurement using the streaming potential method in a cylindrical cell (Surpass from Anton Paar, Graz, Austria). The electrolyte was composed of $10^{-2}$ M NaCl degassed with $N_2$ throughout the experiment and the pH was titrated by either $10^{-2}$ M HCl or $10^{-2}$ M NaOH to explore both the acidic and the alkaline sides of the pH range.

The gold nanoparticles were also analyzed by SEM for morphology and size after deposition of a 3 µL droplet of suspension on a silicon plate. Transmission electron microscopy (TEM, Tecnai Osiris from FEI, Hillsboro, USA) was used for more precise checking of their size distribution. The acceleration voltage was 200 kV. The commercial suspensions were diluted in UP water (dilution factor of 20) and 3 µL were deposited on a copper TEM grid covered with an ultrathin

carbon film supported by a holey carbon film. After drying, the grid was kept in a vacuum chamber until analysis. The size distribution of the particles was processed with ImageJ software (NIH, available at http://rsb.info.nih.gov/ij/). Intensity weighted z-average hydrodynamic diameter ($D_h$) and Zeta potential (ZP) were also assessed using a ZetaSizer Nano ZSP (Malvern Instruments, Worcs, UK) after dilution to 5 mg $L^{-1}$ in $10^{-2}$ M NaCl. $D_h$ and ZP values were measured at pH 7.5 and pH 10, corresponding to the eluent values during the injections and the subsequent desorption assay (see § Column experiment).

SEM observation of AuNP adhesion on the sand was performed without metallization to better locate the nanoparticles in the backscattered electron mode where difference in element atomic number is magnified.

**Column Experiment Protocol**

All experiments were performed at ambient temperature (21 +/- 1 °C).

The set-up used for transport experiments was composed of an inert chromatography pump (IC 25, Dionex, Sunnyvale, USA), an inert 6-way low-pressure injector (Hamilton, Bonaduz, Switzerland) equipped with a 3 mL PTFE injection loop (ca. 6 pore volumes), and the column. For each injection, the sample loop was flushed with 10 mL of sample in the “load” position to ensure homogeneous concentration throughout the loop. The tubing parts were made of PTFE to limit adsorption of the sample as much as possible, and the other parts were made of inert material (PEEK and HDPE) when PTFE was not available. The set-up was hyphenated with an inductively coupled plasma mass spectrometer (ICP-MS, 7700x from Agilent Technologies, Santa Clara, USA) via two T-connectors. The ICP-MS was equipped with a sample introduction PFA inert sapphire kit (micromist PFA nebulizer, low-condensation PFA spray chamber, and sapphire

injector), an o-ring-free quartz torch, Pt-sampler and skimmer cones, and a collision cell (not used in this study). It was either set for monitoring the NP breakthrough curve in a standard time resolved analysis (TRA) mode or in the "single particle" (sp) mode. The experimental conditions for these two modes are listed in Table S1. In standard mode, the monitored isotopes were $^{27}Al$, $^{37}Cl$ (eluent), $^{79}Br$ (conservative tracer, in the sample), $^{89}Y$ (internal standard for Br and Al), $^{195}Pt$ (internal standard for Au), and $^{197}Au$ (solute). Dwell times were adjusted so as to avoid detector saturation and $^{27}Al$ (corrected for by $^{89}Y$ in Figure 5) was added to the list with an integration time calculated so that the total sampling period was equal to one second, including settling time. In the sp mode, only $^{197}Au$ was recorded with the minimum attainable dwell time (3 ms) during one-minute runs. ICP-MS calibration was carried out using ionic gold standards diluted in 0.2% HCl / 0.3% $HNO_3$ (concentration range 2-20 µg $L^{-1}$) and transport efficiency (6%) was calculated according to the number method by injecting an AuNP standard of known size (48 nm) and concentration (50 ng $L^{-1}$). The time scan raw data were converted into particle size distributions using a spreadsheet adapted from the freely downloadable one developed by the RIKILT (the Netherlands) at http://www.wur.nl/en/show/Single-Particle-Calculation-tool.htm.

The eluent ($10^{-2}$ M NaCl at pH 7.5 +/- 0.5) was filtered through a 0.45 µm membrane (Millipore, Burlington, USA). The flow rate of the chromatography pump was set at 0.5 mL $min^{-1}$ (measured value of 0.524 +/- 0.009 mL $min^{-1}$). The ICP-MS uptake rate of the peristaltic pump was measured at 0.354 +/- 0.004 mL $min^{-1}$. The differential flow between the flow rate imposed through the column by the eluent pump and the uptake rate of the ICP-MS was discarded to waste via the first T-connector positioned at the outlet of the column. The external standard for Br and Au (40 µg $L^{-1}$ Y and 100 µg $L^{-1}$ Pt, respectively, in 1% $HNO_3$ and 1% HCl) was introduced into the flow stream

via the second T-connector positioned immediately prior to the nebulizer of the ICP-MS at a flow rate of 0.012 +/-0.001 mL $min^{-1}$ using a second channel of the ICP-MS peristaltic pump head.

The column used in this study was made of glass with a total length of 7 cm and an internal diameter of 0.66 cm (Omnifit, Sigma-Aldrich). At one of the column ends, an adjustable endpiece allowed for choosing the effective length of the packed bed (0 cm to full length). Polymer grids holding a polyamide grid filter of 30 µm pore size (Nytrel-TI quality 30 from UGB, Weert, The Netherlands) embedded in the endcaps prevented the sand from seeping out of the column.

Two grams of dry sand were introduced into the column by one of its ends. To ensure satisfactory saturation of the porous medium, the end caps were fixed in a loose position and the sand column was flushed until all the air bubbles were eluted out. The mobile piston was then moved by screwing it down so that the sand was compressed to its minimum pore volume (corresponding to a bed length of 4 cm). The sand was changed before each experiment, so that no interference due to previous injections might alter the results. For each new sand bed, the porosity was calculated by weighing the empty column, the column containing the dry sand, and the saturated column. The mean porosity was 44 +/- 2%. After the saturation step, the sand column was equilibrated with the eluent for at least 20 min corresponding to ca. 40 pore volumes.

For each set of experiments, injections of the samples (40 µg $L^{-1}$ AuNPs + 150 µg $L^{-1}$ $Br^-$ in $10^{-2}$ M NaCl, pH 7.5) were initially made with a zero-volume column (bed length = 0 cm, joint pistons). They serve as a reference for recovery calculation of the fraction of particles retained on the sand. Then, after filling the column with sand, nine successive identical injections were performed with the same sand bed to check for a possible saturation process of particle retention. After this series of injections, the eluent pH was increased to 10 with NaOH, keeping $10^{-2}$ M NaCl as the background electrolyte. The eluent tubing upstream from the chromatography pump was

rinsed with UP water, flushed with the new alkaline eluent, and connected back to the pump inlet; the same isotopes were monitored in the outflow with the aim of quantifying the release of the particles deposited during the previous nine injections.

All the conditions tested were duplicated and the presented data are expressed as the mean +/- standard deviation of the two identical sets of experiments.

All BTCs are presented as normalized ($S/S_0$) corrected signals according to:

$$S_{Br,corr} = (S_{Br}/C_{Br(sample)})/(S_Y/C_{Y(int\ std)}) \quad \text{(Eq. S1)}$$

$$S_{Au,corr} = (S_{Au}/C_{Au(sample)})/(S_{Pt}/C_{Pt(int\ std)}) \quad \text{(Eq. S2)}$$

With $S_{"M"}$ the raw ICP-MS signal of element "M" (in cps), $C_{"M"(sample)}$ the concentration of element "M" in the sample (in µg $L^{-1}$), and $C_{"M"(int\ std)}$ the concentration of element "M" in the added internal standard (in µg $L^{-1}$). $S_0$ refers to the signal on the plateau of the reference BTC (experiments with joint pistons) and S is the signal of the BTC with the packed sans bed.

The recovery was calculated by the ratio between the area below the BTC of Au obtained with the column filled with sand and that with the column of zero volume.

Concerning the experiments with the ICP-MS in sp mode detection online, the concentration of AuNPs in the sample had to be lowered to reduce the occurrence of particle coincidence detection. The procedure consisted in injecting samples of decreasing AuNP concentration (each injection being performed in a freshly packed column) until the number of detected events was below 5% of the total number of events at the maximum of the breakthrough curve (between 6 min and 7 min). The optimized concentrations were 0.05 µg $L^{-1}$ and 0.5 µg $L^{-1}$ for AuNP-50 nm and AuNP-100 nm, respectively.

For SEM observation of the NP attachment to the sand, a specific experiment was designed. A small column (2.5 cm length x 0.3 cm internal diameter) was filled with the purified sand with the same procedure as described above. The column was flushed with $10^{-2}$ M NaCl prior to injection of 3 mL of AuNP-100 nm 1 mg $L^{-1}$ in $10^{-2}$ M NaCl at a flow rate of 0.1 mL $min^{-1}$. The flow rate was adapted to yield a flow velocity in the column close to that in the column used for the attachment tests. The concentration of AuNPs in the injected sample had to be increased (to 1 mg $L^{-1}$) compared to the concentration used for the attachment tests to detect a significant number of particles on the sand.

**DLVO Theory and Attachment Efficiency**

The Derjaguin-Landau-Verwey-Overbeek (DLVO) theory was used to estimate the total interaction energy between AuNPs and sand grains (Eq. 1 in the main text).

The retarded Hamaker expression was used for the van der Waals interaction energy ($\Phi_{vdW}$):[1, 2]

$$\Phi_{vdW} = -\frac{A_{pwc} d_p}{12h}\left(\frac{1}{1+14\frac{h}{\lambda}}\right) \quad \text{(Eq. S3)}$$

Where $A_{pwc}$ is the Hamaker interaction parameter between the particle and the collector when suspended in water, $h$ is the separation distance, and $\lambda$ is the London characteristic wavelength often assumed to be ca. 100 nm. Hamaker constants were calculated according to the following equation:[3]

$$\mathrm{A}_{pwc} = (\sqrt{A_{cc}} - \sqrt{A_{ww}})(\sqrt{A_{pp}} - \sqrt{A_{ww}}) \quad \text{(Eq. S4)}$$

The Hamaker constants $A_{cc}$ were taken as 8.86 $10^{-20}$ J and 1.52 $10^{-19}$ J for quartz and alumina, respectively, and $A_{ww}$ was taken as 3.70 $10^{-20}$ J.[4] $A_{pp}$ (3.46 $10^{-19}$ J for gold) was deduced from $A_{pwp}$

191 $(2.70\ 10^{-19}\ J)^3$ and $A_{ww}$. The Hamaker constant for the edge surface of kaolinite was taken as 1.20

192 $10^{-19}$ J.[5]

193 The electrostatic interaction energy ($\Phi_{El}$) was calculated using the following sphere-plane

194 expression valid for 1:1 electrolytes and surface potentials less than 60 mV:[2, 6]

195 $$\Phi_{El} = \pi\varepsilon_0\varepsilon_r \frac{d_p}{2}\left(2\psi_p\psi_c ln\left[\frac{1+exp(-\kappa h)}{1-exp(-\kappa h)}\right] + (\psi_p{}^2 + \psi_c{}^2) ln[1 - exp(-2\kappa h)]\right) \quad \text{(Eq. S5)}$$

196 Where $\varepsilon_0$ is the vacuum permittivity, $\varepsilon$ is the dielectric constant of the medium, $\Psi_p$ and $\Psi_c$ are

197 the surface potentials of the particle and the collector, respectively (approximated by the

198 corresponding zeta potentials), and κ is the Debye-Hückel parameter.

199 The short-range Born repulsion between a sphere and a plate reflecting the overlap of electron

200 orbitals was expressed as:[7]

201 $$\Phi_{Born} = \frac{A_{pwc}\sigma_B^6}{7560}\left(\frac{4d_p+h}{(d_p+h)^7} + \frac{3d_p-h}{h^7}\right) \quad \text{(Eq. S6)}$$

202 Where $\sigma_B$ is the Born collision diameter taken as 0.5 nm.[2]

203 The DLVO interaction between two clay platelets (alumina face-silica face) or between a clay

204 platelet (alumina face) and the sand grain (silica) in the suspending medium (water) was described

205 by:

206 $$\Phi_{tot} = \Phi_{vdW} + \Phi_{El} + \Phi_{rep} \quad \text{(Eq. S7)}$$

207 With the expressions of $\Phi_{vdW}$ and $\Phi_{El}$ between two planar surfaces:[5, 8]

208

209 $$\Phi_{vdW} = -\frac{A_{AwS}}{12\pi}\left(\frac{1}{h^2}\right) \quad \text{(Eq. S8)}$$

210 $$\Phi_{El} = \varepsilon_0\varepsilon_r\kappa\left(\frac{2\psi_p\psi_c exp(\kappa h) - \psi_p{}^2 - \psi_c{}^2}{exp(2\kappa h) - 1}\right) \quad \text{(Eq. S9)}$$

211 Where $A_{AwS}$ represents the Hamaker constant for the interaction between the two minerals

212 (alumina and silica faces) in water $(2.08\ 10^{-20}\ J)$[5].

The short-range hydration repulsive energy was accounted for by the empirical expression:

$$\Phi_{rep} = \Phi_0 e^{-h/\sigma} \quad \text{(Eq. S10)}$$

Where $\Phi_0 = k_B T/\sigma^2$ and $\sigma$ was taken as the diameter of the water molecule (0.343 nm).

As already mentioned in the literature, DLVO theory cannot describe particle deposition onto a heterogeneous surface adequately, and experimentally determined zeta potentials do not reflect the surface potential of local mineral structures.[9] That is why the surface potential used here for calculations of the interactions between kaolinite and gold nanoparticles was not approximated by the measured zeta potential of the sand but taken from the literature.

The data used for DLVO calculations reported hereafter are given in Table S2.

The equation proposed by Tufenkji and Elimelech was used for the calculation of the single-collector contact efficiency $\eta_0$:[10]

$$\eta_{0=} 2.44\, A_s^{1/3} N_R^{-0.081} N_{Pe}^{-0.715} N_{vdW}^{0.052} + 0.55 A_s N_R^{1.675} N_A^{0.125} + 0.22 N_R^{-0.24} N_G^{1.11} N_{vdW}^{0.053} \quad \text{(Eq. S11)}$$

$A_s$ is defined as:

$$A_s = \frac{2(1-\gamma^5)}{2-3\gamma+3\gamma^5-2\gamma^6} \quad \text{(Eq. S12)}$$

Where $\gamma = (1-\varepsilon)^{1/3}$ and $\varepsilon$ is the porosity of the porous medium.

$N_R$ is the aspect ratio, $N_{Pe}$ is the Peclet number, $N_{vdW}$, $N_A$, and $N_G$ are the van der Waals, the attraction, and the gravity numbers, respectively.

## Additional Tables and Figures

**Table S1.** ICP-MS experimental conditions

| | Standard mode | « sp » mode |
|---|---|---|
| RF power (W) | 1550 | |
| Plasma gas (Ar) flow rate (L $min^{-1}$) | 15 | |
| Nebulizer gas (Ar) flow rate (L $min^{-1}$) | 1.15 | |
| Integration time / mass (s) | $^{27}Al$ : 0.67<br>$^{37}Cl$ : 0.003<br>$^{79}Br$ 0.01<br>$^{89}Y$: 0.1<br>$^{195}Pt$: 0.1<br>$^{197}Au$ : 0.1 | $^{197}Au$: 0.003 |

**Table S2.** Hamaker constants and surface potentials used for interaction energy profile calculation according to the DLVO model

| Interaction (1)-water-(2) | Hamaker constant (J) | Potential (1) (mV) | Potential (2) (mV) |
|---|---|---|---|
| 50 nm AuNP-water-sand grain, pH 7.5 100 nm | $5.47\ 10^{-20}$ (1) | -43.7 (3) -47.8 (3) | -55 (5) |
| 50 nm AuNP-water-sand grain, pH 10.0 100 nm | $5.47\ 10^{-20}$ (1) | -45.1 (3) -49.4 (3) | -85 (5) |
| 50 nm AuNP-water-kaolinite (edge), pH 7.5 100 nm | $8.01\ 10^{-20}$ (1) | -43.7 (3) -47.8 (3) | -2 (4) |
| 50 nm AuNP-water-kaolinite (edge), pH 10.0 100 nm | $8.01\ 10^{-20}$ (1) | -45.1 (3) -49.4 (3) | -37 (4) |
| Alumina face-water-silica face, pH 7.5 | $2.08\ 10^{-20}$ (2) | -2 (4) | -37 (4) |
| Alumina face-water-silica face, pH 10.0 | $2.08\ 10^{-20}$ (2) | -37 (4) | -37 (4) |

(1)Calculated from Eq. S4, (2)From [5], (3)From Table S3, (4)From [11], (5)From Figure S2

The potential of quartz was taken from Figure S2 because the experimental zeta potential is dominated by that of the highly predominant quartz phase. The other potentials (kaolinite edge, alumina and silica faces) were not accessible in the course of this study and were therefore taken from the literature.

**Table S3.** Characteristics of the gold nanoparticles. TEM mean diameter ($D_{TEM}$), DLS mean hydrodynamic diameter ($D_h$), polydispersity (PDI), zeta potential (ZP), and average mass-based diameter from spICP-MS ($D_{spICP-MS}$). DLS conditions: AuNPs 5 mg $L^{-1}$ in $10^{-2}$ M NaCl. pH adjusted with NaOH. Measurements in triplicate.

| | $D_{TEM}$ (nm) | $D_h$ (nm) | PDI | ZP (mV) | $D_{spICP-MS}$ (nm) |
|---|---|---|---|---|---|
| AuNP-50 nm | 47.5 +/- 3.6 | | | | 49.4 +/- 0.7 |
| pH 7.5 | | 54.4 +/- 0.2 | 0.23 +/- 0.01 | -43.7 +/- 1.9 | |
| pH 10 | | 55.6 +/- 0.6 | 0.21 +/- 0.01 | -45.1 +/- 2.0 | |
| AuNP-100 nm | 110.2 +/- 6.4 | | | | 108.2 +/- 0.4 |
| pH 7.5 | | 108.8 +/- 0.7 | 0.05 +/- 0.02 | -47.8 +/- 1.6 | |
| pH 10 | | 112.4 +/- 0.6 | 0.08 +/- 0.01 | -49.4 +/- 1.1 | |

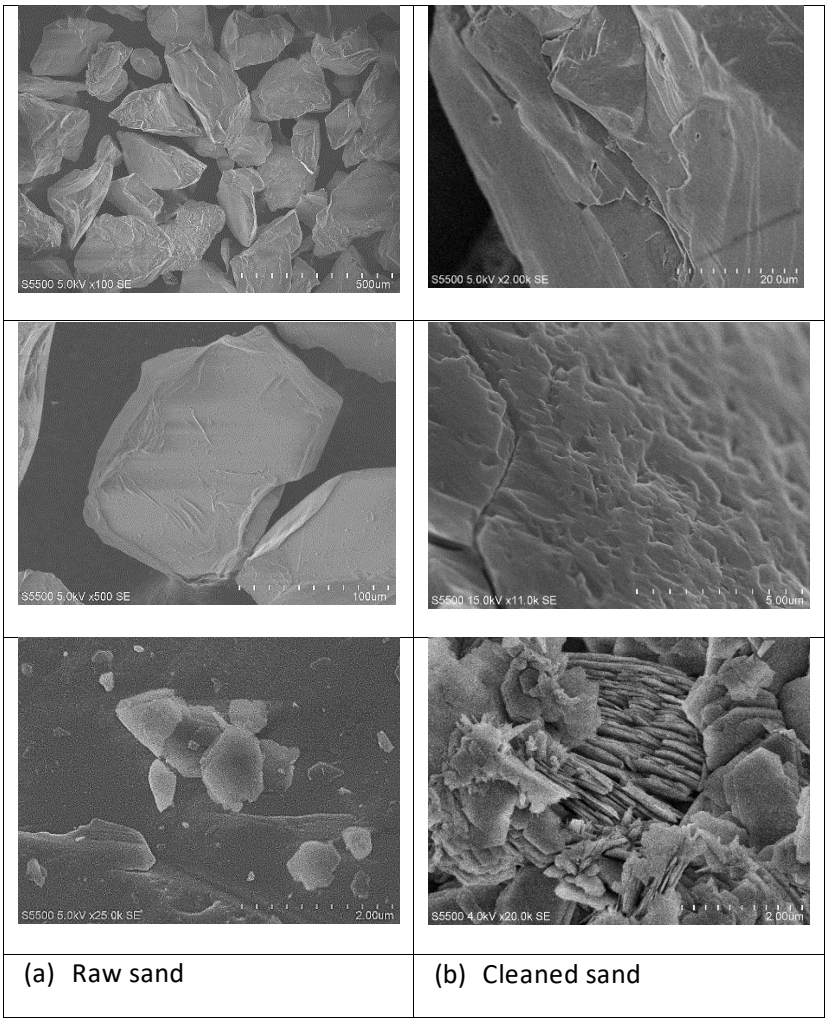


**Figure S1.** SEM follow up on the cleaning process of the Hostun sand. Images of (a) the raw sand and (b) the cleaned sand. Top and middle panels refer to the quartz grains (major constituent of the sand) and bottom images focus on the secondary mineral phase (kaolinite).

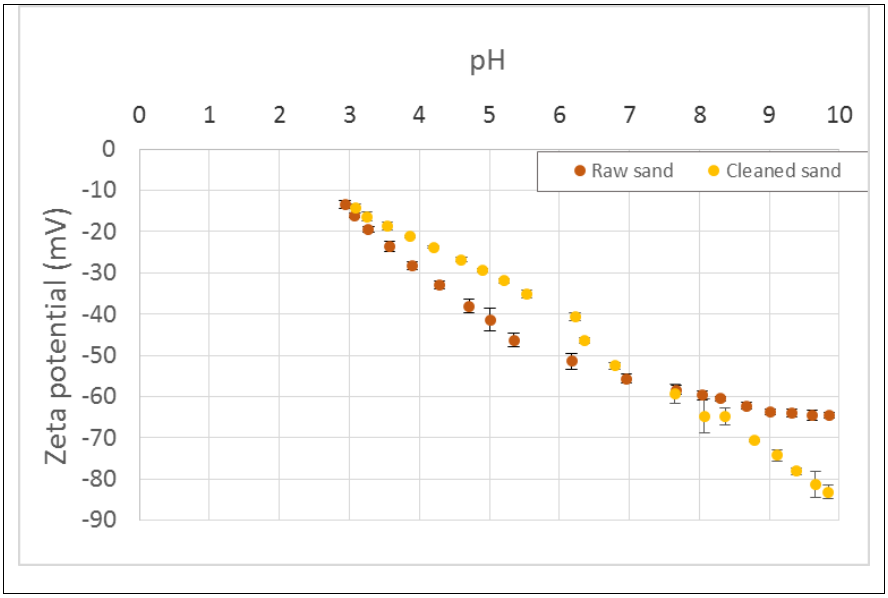


**Figure S2.** Evolution of the zeta potential of the Hostun sand with pH before and after the cleaning process. Background electrolyte: $10^{-2}$ M NaCl.

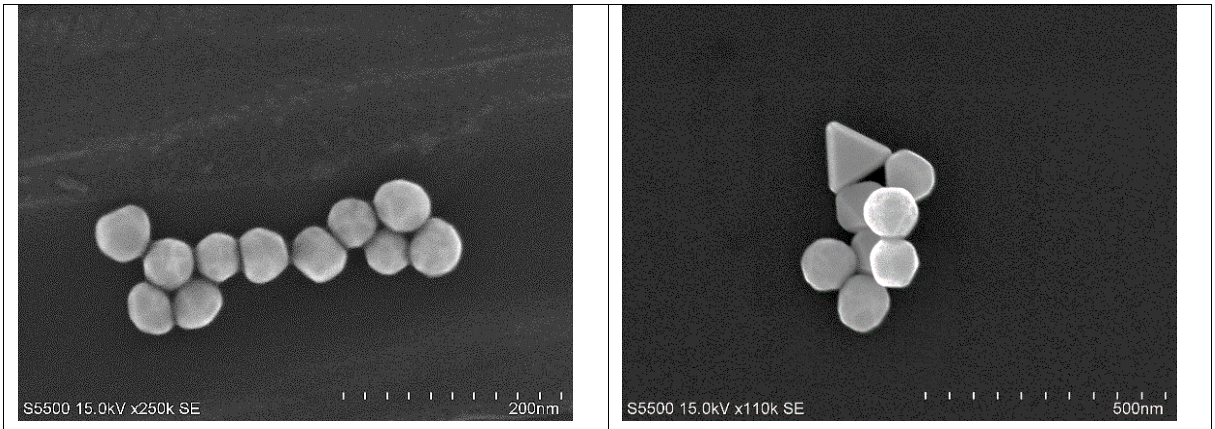


(a) (b)

**Figure S3.** SEM images of the gold nanoparticles. (a): AuNP-50 nm and (b): AuNP-100 nm.

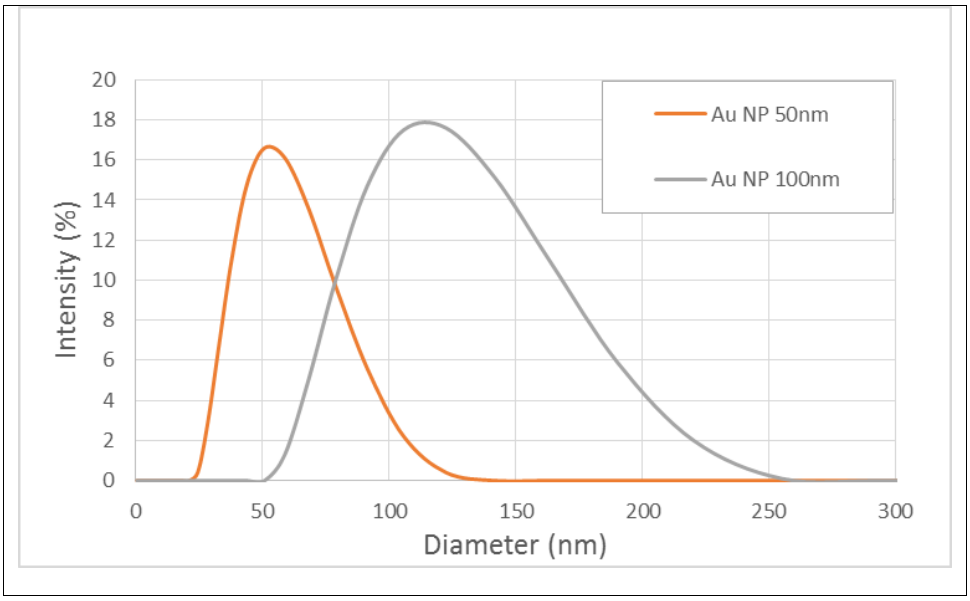


**Figure S4**. Size distribution of the AuNPs determined by DLS. Background electrolyte: $10^{-2}$ M NaCl, pH 7.5.

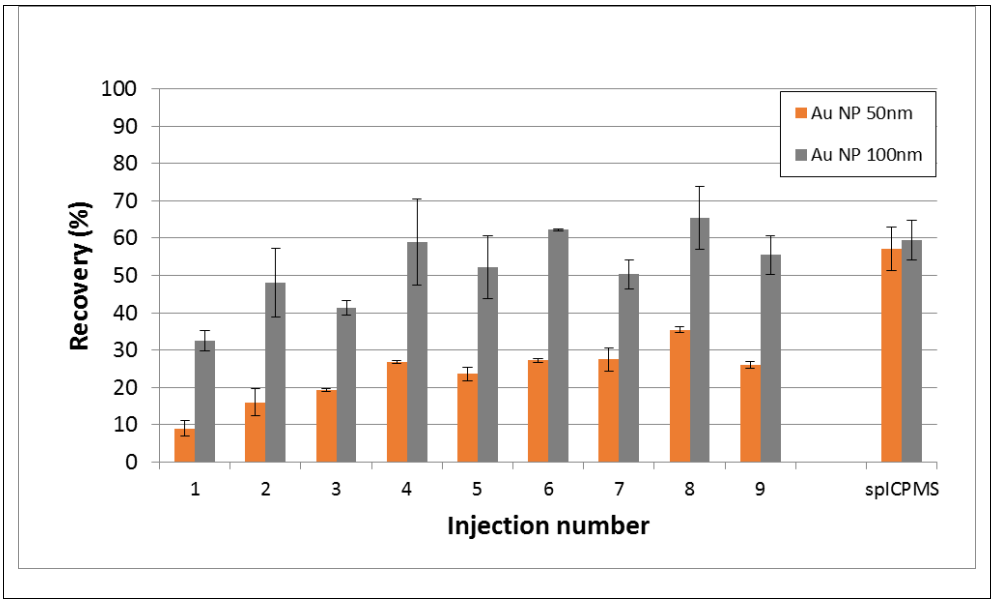


**Figure S5.** Au recovery (mass-based) in the effluent of the column for each successive injection. Sample: AuNPs 40 µg $L^{-1}$ in $10^{-2}$ M NaCl, pH 7.5. Eluent: $10^{-2}$ M NaCl pH 7.5. Flow rate: 0.5 mL $min^{-1}$ (Darcy velocity: 0.026 cm $s^{-1}$). Error bars correspond to twice the standard deviation of the duplicated experiments.

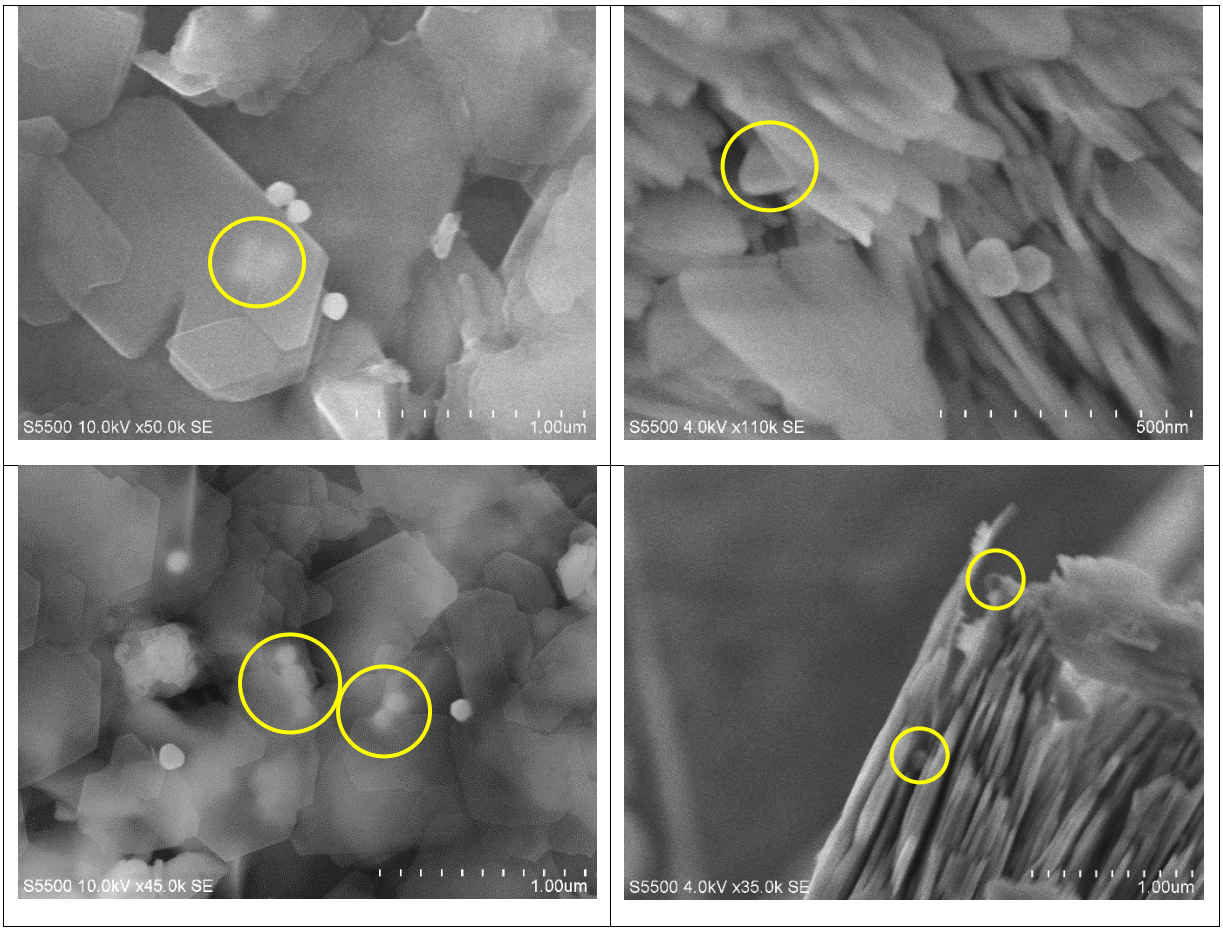


279 **Figure S6.** SEM images of AuNP-100 nm attached on kaolinite. AuNPs are preferably located on
280 edges of the clay platelets or entrapped within the stacks between sheets. Yellow circles point at
281 these "hidden" particles.

282

283

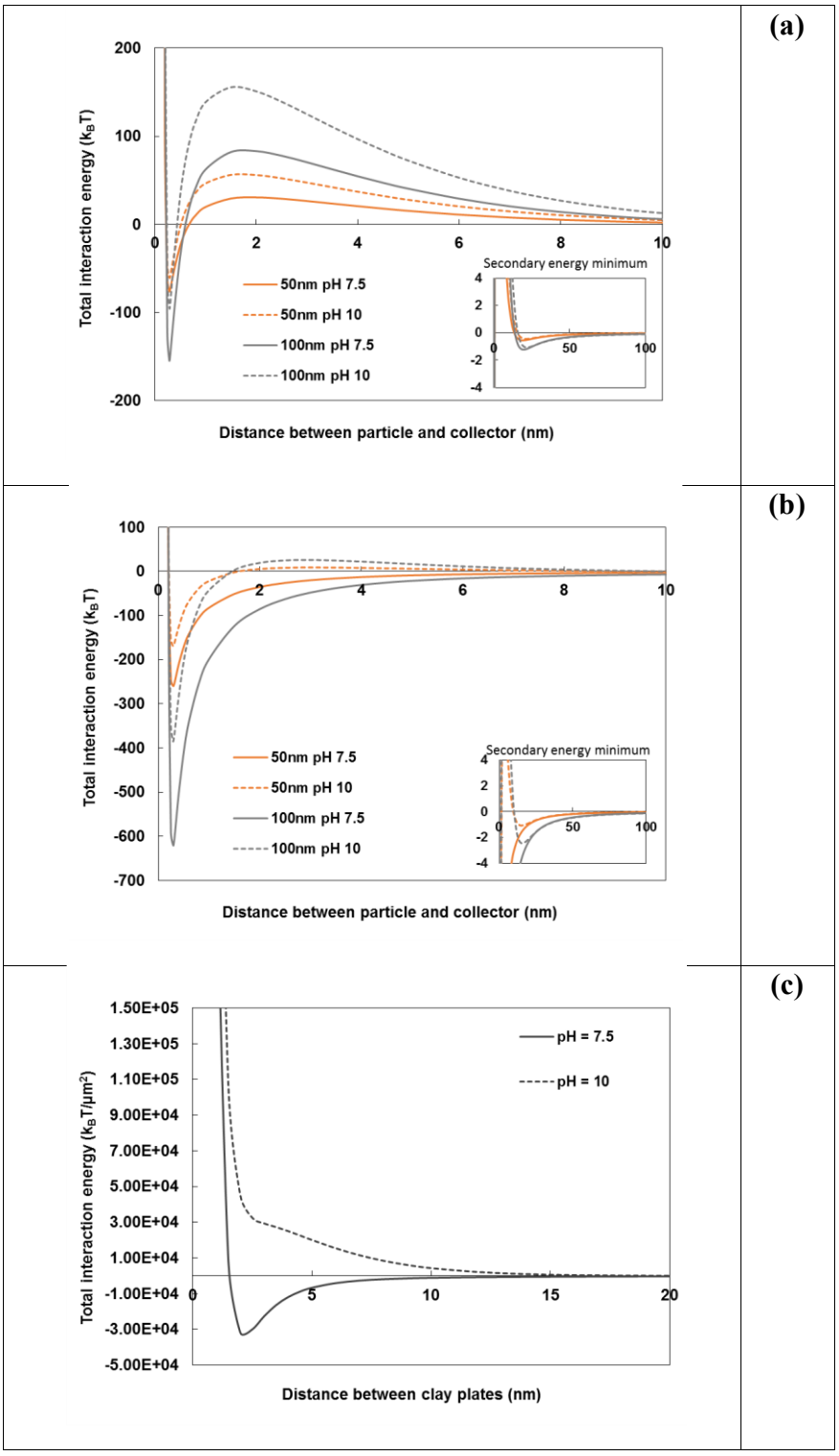


284 **Figure S7.** Calculated DLVO interaction energy profiles between (a) a gold NP and a flat quartz
285 surface, (b) a gold NP and the edge of a kaolinite sheet for both NP sizes (50 nm and 100 nm), and
286 (c) a flat alumina face and a flat silica face. The curves are drawn at pHs of both attachment (pH

287 7.5) and detachment (pH 10) experiments. Inserts correspond to the close-up view of secondary
288 energy minima.

289

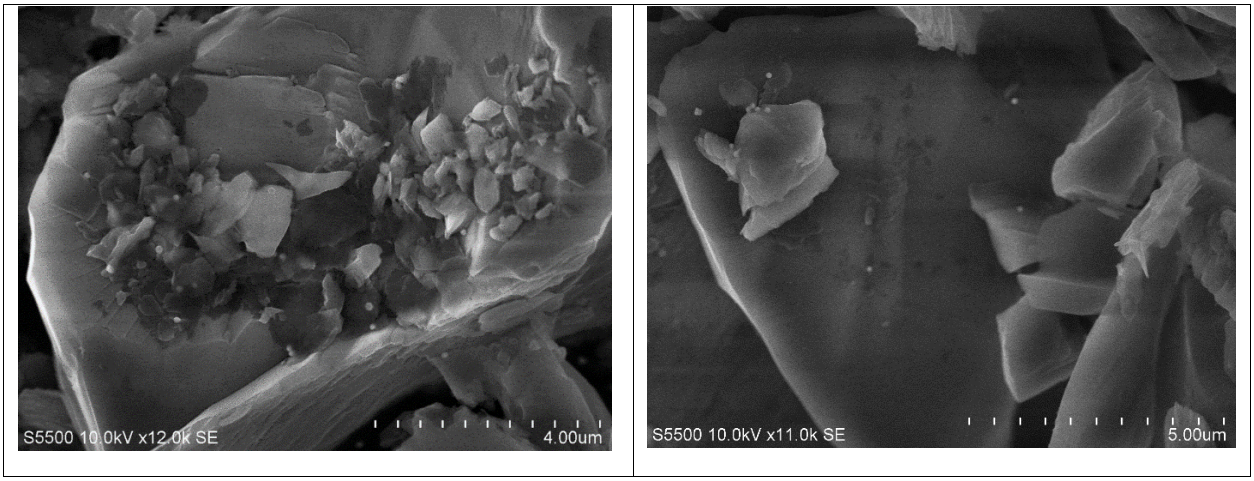


290 **Figure S8.** General views of AuNP-100 nm attached on the collector (quartz sand grain with
291 kaolinite platelets on the surface) by SEM imaging. Note the preferred location of AuNPs on the
292 clay platelets.

293 REFERENCES


294 1. Gregory, J., Approximate expressions for retarded van der waals interaction. *Journal of*
295 *Colloid and Interface Science* **1981,** *83*, (1), 138-145.
296 2. Hahn, M. W.; Abadzic, D.; O'Melia, C. R., Aquasols: On the Role of Secondary Minima.
297 *Environmental Science & Technology* **2004,** *38*, (22), 5915-5924.
298 3. Petosa, A. R.; Jaisi, D. P.; Quevedo, I. R.; Elimelech, M.; Tufenkji, N., Aggregation and
299 Deposition of Engineered Nanomaterials in Aquatic Environments: Role of Physicochemical
300 Interactions. *Environmental Science & Technology* **2010,** *44*, (17), 6532-6549.
301 4. Bergström, L., Hamaker constants of inorganic materials. *Advances in Colloid and*
302 *Interface Science* **1997,** *70*, 125-169.
303 5. Gupta, V.; Hampton, M. A.; Stokes, J. R.; Nguyen, A. V.; Miller, J. D., Particle interactions
304 in kaolinite suspensions and corresponding aggregate structures. *Journal of Colloid and Interface*
305 *Science* **2011,** *359*, (1), 95-103.
306 6. Redman, J. A.; Walker, S. L.; Elimelech, M., Bacterial Adhesion and Transport in Porous
307 Media: Role of the Secondary Energy Minimum. *Environmental Science & Technology* **2004,** *38*,
308 (6), 1777-1785.
309 7. Ruckenstein, E.; Prieve, D. C., Adsorption and desorption of particles and their
310 chromatographic separation. *AIChE Journal* **1976,** *22*, (2), 276-283.
311 8. de Kretser, R. G.; Scales, P. J.; Boger, D. V., Surface chemistry-rheology inter-
312 relationships in clay suspensions. *Colloids and Surfaces A: Physicochemical and Engineering*
313 *Aspects* **1998,** *137*, (1), 307-318.
314 9. Lin, S.; Cheng, Y.; Bobcombe, Y.; L. Jones, K.; Liu, J.; Wiesner, M. R., Deposition of
315 Silver Nanoparticles in Geochemically Heterogeneous Porous Media: Predicting Affinity from
316 Surface Composition Analysis. *Environmental Science & Technology* **2011,** *45*, (12), 5209-5215.
317 10. Tufenkji, N.; Elimelech, M., Correlation Equation for Predicting Single-Collector
318 Efficiency in Physicochemical Filtration in Saturated Porous Media. *Environmental Science &*
319 *Technology* **2004,** *38*, (2), 529-536.
320 11. Williams, D. J. A.; Williams, K. P., Electrophoresis and zeta potential of kaolinite. *Journal*
321 *of Colloid and Interface Science* **1978,** *65*, (1), 79-87.


322

323